JOURNAL OF PROPULSION AND POWER
Vol. 21, No. 3, May–June 2005

Comparison of Mixing Characteristics of Unlike Triplet Injectors Using Optical Patternator

Kihoon Jung,* Byoungjik Lim,† and Youngbin Yoon‡
Seoul National University, Seoul 151-742, Republic of Korea
and
Ja-Ye Koo§
Hankuk Aviation University, Kyunggi-Do 412-791, Republic of Korea

Mixing characteristics of an unlike split triplet fuel–oxidizer–oxidizer–fuel (F–O–O–F) injector, which separates the single oxidizer hole of an unlike triplet fuel–oxidizer–fuel (F–O–F) injector for liquid-rocket engines, were investigated under cold-flow conditions. The spray mass distributions of the fuel and oxidizer were measured using an optical patternator based on the planar liquid laser-induced fluorescence technique, and the mixing mechanism and the mixing efficiency of the F–O–O–F injector were compared with those of the F–O–F injector. Results showed that the mixing efficiency of the F–O–O–F injector is less sensitive to the changes of the momentum ratio or impingement angle than that of the F–O–F injector because the mixing of the F–O–O–F injector is determined by the coalescing process of two liquid sheets, whose impinging momentum is weak. Therefore, the F–O–O–F injector has an advantage in starting injection wherein the momentum ratio is usually different from the operating condition.

Nomenclature

DI	=	index of deviation from injection mass flow rate
d	=	orifice diameter
E_m	=	mixing efficiency, %
G	=	gray level of fluorescence signal
I_i	=	averaged intensity of incident laser beam
K	=	constant
$\dot{M}$	=	total mass flow rate injected from orifice hole(s) or fuel holes
$\dot{m}$	=	mass flow rate of spray passing local cell
n	=	number of pixels where $r \leq R$
$\bar{n}$	=	number of pixels where $r > R$
R	=	total mixure fraction of fuel and oxidizer, $\dot{M}_o/(\dot{M}_o + \dot{M}_f)$
R_M	=	momentum ratio of oxidizer to fuel, $\dot{M}_o V_o/\dot{M}_f V_f$
r	=	local mixture fraction of fuel and oxidizer, $\dot{m}_o/(\dot{m}_o + \dot{m}_f)$
V	=	injection velocity
$\bar{V}_d$	=	averaged radial velocity of drops
V_z	=	z-axial component of spray velocity
Z_1	=	distance from injector surface to measurement location
Z_2	=	distance from last impingement point to measurement location
θ	=	one-half impingement angle, angle between fuel and oxidizer orifices
μ	=	dynamic viscosity
ρ	=	liquid density
$\bar{\rho}$	=	time-averaged spray density
σ	=	surface tension

Subscripts

f	=	fuel
o	=	oxidizer

Received 10 February 2003; accepted for publication 10 July 2004.

*Ph.D., School of Mechanical and Aerospace Engineering.
†Master, School of Mechanical and Aerospace Engineering.
‡Professor, School of Mechanical and Aerospace Engineering, San 56-1, Shinlim-dong, Kwanak-ku; ybyoon@snu.ac.kr.
§Professor, School of Aerospace and Mechanical Engineering.

I. Introduction

UNLIKE-TRIPLET oxidizer–fuel–oxidizer (O–F–O) or fuel–oxidizer–fuel (F–O–F) injectors are commonly used in liquid rocket engines that use liquid oxygen (LOX) and hydrocarbon propellants because of their operational reliability and potentially high mass flow rates. In particular, the O–F–O injector has been known as the best impinging-type injector with regard to both combustion performance and stability.[1–4] However, it has poor wall compatibility, and, thus, the F–O–F injector has been used when the wall compatibility is more important than combustion performance.[3,4]

The maximum specific impulse of LOX/kerosene propellant can be obtained when the optimum mixture ratio is approximately 2.3 (Ref. 5). To satisfy this mixture ratio, the area of oxidizer hole of the F–O–F injector has to be about three times as large as that of the fuel hole.[4,6] Because the large difference between the oxidizer and fuel hole diameters may reduce the atomization efficiency, a fuel–oxidizer–oxidizer–fuel (F–O–O–F) (or unlike-split-triplet) injector, which separates the single oxidizer hole of the F–O–F injector into double oxidizer holes, was designed.[6,7]

Pavli[6] reported from his subscale engine tests that the combustion performance of the F–O–O–F injector is as high as that of the O–F–O injector, whereas that of a pair of like-doublet [fuel–fuel (F–F) and oxidizer–oxidizer (O–O)] injectors is relatively low. Although the hot test definitely showed the high combustion performance of the F–O–O–F injector, it was difficult to find the fundamental reasons for this high performance because the atomization or mixing mechanism of liquid propellants could not be investigated under combustion conditions.

In general, poor performance of an injector at cold-flow conditions leads to poor combustion performance of the injector, although high performance at cold-flow conditions does not imply high combustion performance.[4] As for the cold-flow tests, Won et al.[7] compared the mixing efficiencies of F–O–O–F, oxidizer–fuel–fuel–oxidizer (O–F–F–O), and unlike-doublet fuel–oxidizer (F–O) injectors. From the results, they found that the mixing efficiency of the F–O–O–F injector is the highest for the same momentum ratios. However, the comparison between the F–O–O–F and F–O–F injectors has not been reported, even though the F–O–O–F injector has been modified from the F–O–F injector. In the present study, therefore, the spray mixing characteristics of the F–O–O–F injector were investigated and compared with those of the F–O–F injector under cold-flow conditions.

To study the mixing characteristics of liquid propellants, both mass distributions of oxidizer and fuel have to be measured. As

a measurement technique for the mass distribution, a mechanical patternator, which collects the injected spray mass at many cells during a specified time, is used.[7,8] However, this method has several limitations: low spatial resolution, measurement inconvenience, disturbance to the spray, and so on. As a nonintrusive optical patternator, a phase Doppler particle analyzer, (PDPA), which measures both the sizes and velocities of spherical drops using light scattering interferometry, can obtain very reliable mass flux data.[9] However, the PDPA is difficult to apply to a dense spray zone, which contains nonspherical drops and multiple particles.[10] In contrast, a planar liquid laser-induced fluorescence (PLLIF) technique, which is based on the linearity of the fluorescence signal to the spray mass concentration, can obtain two-dimensional mass distributions with high spatial resolution, regardless of whether the drops are spherical or not.[11] Because the present sprays of the F–O–O–F and F–O–F injectors include liquid sheets or ligaments, as well as fine drops at the measurement locations, we used the optical patternator based on the PLLIF technique instead of the PDPA.

II. Experimental Methods

A. PLLIF Basics and Its Validation

The PLLIF technique is based on the fluorescence signal intensity being proportional to the concentration of fluorescence molecules under the condition that the laser light absorption is low enough for the molecules to be uniformly illuminated.[12] Thus, the gray level of fluorescence signal at a charge-coupled device pixel of (x, y) location can be described as follows[10]:

$$G(x, y) = K I_i(x, y)\bar{\rho}(x, y) \tag{1}$$

where $\bar{\rho}(x, y)$ indicates the time-averaged spray density during the camera exposure time, and, thus, the gray level in Eq. (1) indicates the total spray mass that does not pass but that exists at the corresponding volume of the pixel area and the beam thickness during the exposure time, that is, the spatial spray mass concentration. Furthermore, the constant K is difficult to obtain, and so the gray levels can give only qualitative data. Consequently, Eq. (1) indicates that only the relative distribution of spatial spray mass concentration can be obtained from the PLLIF measurement.

To validate the linearity of the fluorescence signal to the concentration of fluorescent molecules, an experiment was carried out as shown in Fig. 1a. An Ar–ion laser sheet beam illuminated a quartz cell filled with the same liquid solution as the fuel or oxidizer simulant. A blocking slit was used to minimize the secondary emission by nearby fluorescence molecules. Figure 1b shows the gray levels of the fluorescence signals as a function of the fluorescent dye concentration; symbols and error bars indicate the averaged values for 100 data points and their standard deviations, respectively, and the maximum level is 255 because the 12-bit gray levels were converted into 8-bit form, which is easier to handle. The gray levels increase linearly as the concentration of fluorescent molecules increases. Therefore, the fluorescence signal is proportional to the spray mass only if the fluorescent molecules are uniformly distributed inside the spray mass.

The result of Fig. 1b also shows that the PLLIF technique can be valid for measuring the liquid-phase mixing. If fluorescent dye of 30 mg/l is added to water to measure the fuel mass distribution, and this mixture is mixed with the oxidizer of pure water at a unit volume, the concentration of fluorescent dye may be determined by the remaining fuel mass at the unit volume. Because the fluorescence signal changes linearly to the dye concentration as shown in Fig. 1b, the signal may show the corresponding level of the fuel mass concentration qualitatively. If it is assumed that the mixing process is steady, the qualitative oxidizer mass distribution also can be measured with the same procedure, using the fluorescent dye solution for the oxidizer simulant and pure water for the fuel simulant.

The qualitative spray mass concentration can be converted into the quantitative local mass flow rate by the following equation[13]:

$$\dot{m}(x, y) = \frac{V_z(x, y)G(x, y)}{\sum_{x,y} V_z(x, y)G(x, y)} \cdot (\dot{M}_o + \dot{M}_f) \tag{2}$$

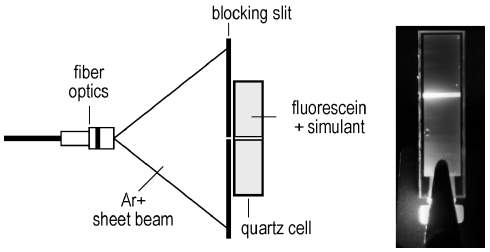

a) Schematic of experimental setup

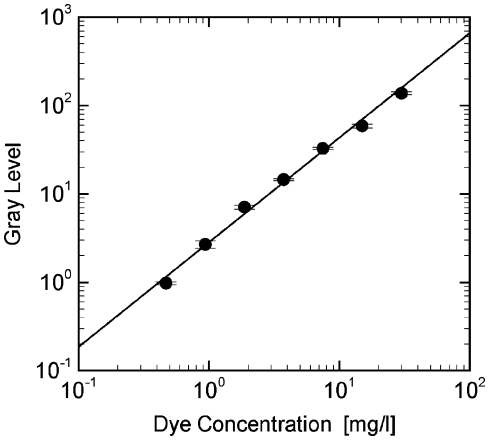

b) Gray levels of fluorescence signals as a function of the dye concentration

Fig. 1 Validation of the linearity of gray levels of fluorescence signals to the dye concentration; error bars in Fig. 1b indicate standard deviations of 100 data points.

where the injection mass flow rate $\dot{M}_o$ or $\dot{M}_f$ can be measured easily, but where it is difficult to obtain the z component of the spray mass velocity V_z because most of the examined sprays do not consist of spherical drops and the PDPA cannot measure the velocities of nonspherical drops. However, if the drops are considered to be distributed almost on spherical surfaces, whose centers are the last impingement points,[14] V_z at each (x, y, z) point can be obtained as follows:

$$V_z(x, y, z) = \bar{V}_d\left(z\Big/\sqrt{x^2 + y^2 + z^2}\right) \tag{3}$$

where $\bar{V}_d$ is an averaged radial velocity of drops on a spherical surface. Finally, the spray mass flow rate distributions of the present injectors can be obtained quantitatively by substituting Eq. (3) for Eq. (2).

B. Experimental Setup for PLLIF Measurements

Figure 2 shows a schematic of the experimental setup for the measurement of the spray mass distributions on the transverse plane using the PLLIF technique. A continuous beam of Ar–ion laser (LEXEL, Model 95) was spread as a sheet beam by a fiber optic beam expander. The mixture of water and methyl alcohol (of volumetric ratio 4:1) was used as simulants of fuel and oxidizer, and Fluorescein ($C_{20}H_{12}O_5$, Aldrich Chemical Company) of 30 mg was dissolved into the simulant of 1 liter. Because the Fluorescein absorbs light in the wavelength range from 400 to 530 nm with the peak wavelength at about 488 nm, the Ar–ion laser beam of 488 nm in wavelength was used. The emission spectrum of the Fluorescein in the present simulant was measured using a monochromator, and it was found that the spectrum ranged from 500 to 650 nm and that the peak emission appears at 525 nm.

After being separated from the scattering signal by an edge filter that cuts off wavelengths below 550 nm, the fluorescence signal was recorded on a digital camera (Canon D30, 12-bit, 2160 × 1440 resolution). The exposure time of the camera was 0.25 s, adequate for temporal averaging, and 50 images were averaged to represent one experimental case. Temporal averaging was large because the

PLLIF technique for the liquid-phase mixing can be used only in steady flows, although the spray flow is unsteady. As shown in Fig. 2, because it was impossible to take images at a normal direction to the sheet beam due to obstruction from the spray, the location of the camera was inclined at about a 40-deg angle, and the perspective errors of the images were corrected by an image transformation method.[10] In addition, generally, both the incident laser sheet beam and the fluorescence signal are scattered as they pass the dense spray, which results in the reduction of fluorescence signal intensity.[11] However, the scattering was not important in the present sheet shape sprays, which have narrow spray zones.[13]

C. Injector Design and Experimental Conditions

The F–O–O–F injector has two oxidizer jets, that are injected in parallel at the injector center and two adjacent fuel jets, that are injected with a specific angle θ, as shown in Fig. 3. The oxidizer and fuel jets impinge at the first impingement points and form two liquid sheets. After the first impingements, the two liquid sheets impinge again at the second impingement location because the sheet angles are not parallel to the center. Although the spray structure of the F–O–O–F injector is similar to that of a pair of unlike-doublet [F–O and oxidizer–fuel (O–F)] injectors, the momentum of the F–O–O–F injector at the second impingement point is stronger, and, consequently, both the atomization and mixing performances of the F–O–O–F injector are better than those of the pair of unlike-doublet injectors.[7] In contrast, the two fuel jets and the oxidizer jet of an F–O–F injector impinge only at the first impingement point and form a single liquid sheet on the x–z plane, which is normal to the y–z plane of liquid jets as shown in Fig. 3.

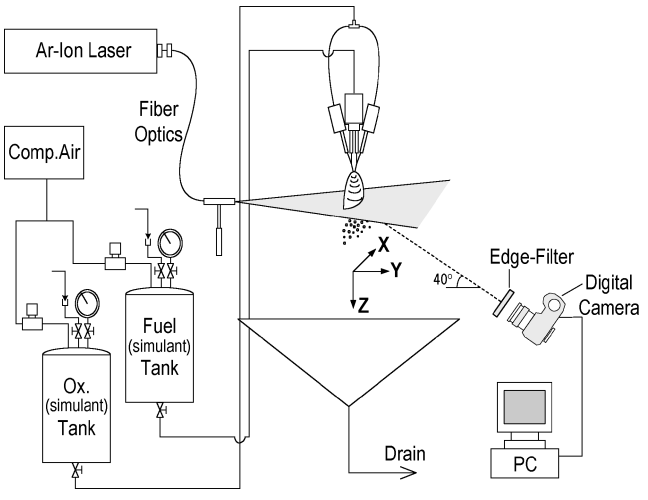

Fig. 2 Schematic of experimental setup for measurements of mass distributions using PLLIF technique.

According to Riebling, the optimum diameter ratio of the F–O–F injector for the maximum mixing efficiency can be obtained by the following correlation[15]:

$$(d_o/d_f)^2_{\mathrm{MME}} = 1.58\left[(\rho_f/\rho_o)(\dot{M}_o/\dot{M}_f)^2\right]^{0.57} \tag{4}$$

Thus, we determined the orifice diameters of the F–O–F injector for the mixture ratio of 2.3 considering Eq. (4) as shown in Fig. 3, that is, $d_o = 1.8$ mm and $d_f = 1.1$ mm. The orifice diameters of the two oxidizer jets of the F–O–O–F injector ($d_o = 1.3$ mm) were designed to have the same cross-sectional area as one oxidizer jet of the F–O–F injector. The ratios of the orifice length to diameter (about 30) were designed to be longer than those of practical injectors (about 5) to reduce deviations in measurements because the longer orifice has been known to make a steadier spray pattern.[14] The impingement angle 2θ, which is defined by the angle between two fuel orifices, was designed to be 30, 45, and 60 deg. As the angle increases, the impinging momentum of fuel jet to the oxidizer jet increases, and, thus, the atomization performance of the injector increases, but the spray zone approaches the injector surface, which can damage the injector under combustion conditions. Although, in general, the unlike-impinging-type injectors have maximum combustion performance when their impingement angles are 60 deg (Refs. 1 and 3), the angles must be decreased when the reduction of heat transfer from the combustion zone to the injector surface is more important than the combustion performance. Therefore, the experimental cases with lower impingement angles of 30 and 45 deg were included to investigate the effect of impingement angle on the mixing performance.

The momentum ratio of oxidizer to fuel R_M was used as a major independent variable, and it was changed from 0.5 to 6.5; the design momentum ratio for the mixture ratio of 2.3 was 3.0. Table 1 shows the experimental conditions for both injectors. We controlled the mass flow rate of the oxidizer under the constant mass flow rate of the fuel to satisfy the momentum ratio based on LOX/kerosene propellant with the present liquid simulants.

As a liquid simulant, a water-based solution, obtained by combining methyl alcohol of 20% of total liquid volume and fluorescent dye, was used to obtain the fluorescence signal. Although, generally, the combination of water/kerosene is used instead of LOX/kerosene propellants in nonreactive tests,[4,7] kerosene has too weak a fluorescence signal and cannot dissolve fluorescein dye; therefore, kerosene cannot be used for the present PLLIF measurements. Because the physical properties of the present simulant ($\rho = 0.8$ g/cm^3, $\sigma = 26$ g/s^2, and $\mu = 0.016$ g/cm $\cdot$ s) are different from those of kerosene ($\rho = 1.0$ g/cm^3, $\sigma = 63$ g/s^2, and $\mu = 0.008$ g/cm $\cdot$ s), we tried to confirm that the similarity of momentum ratio can simulate the real propellant combination. Figure 4 shows the mass

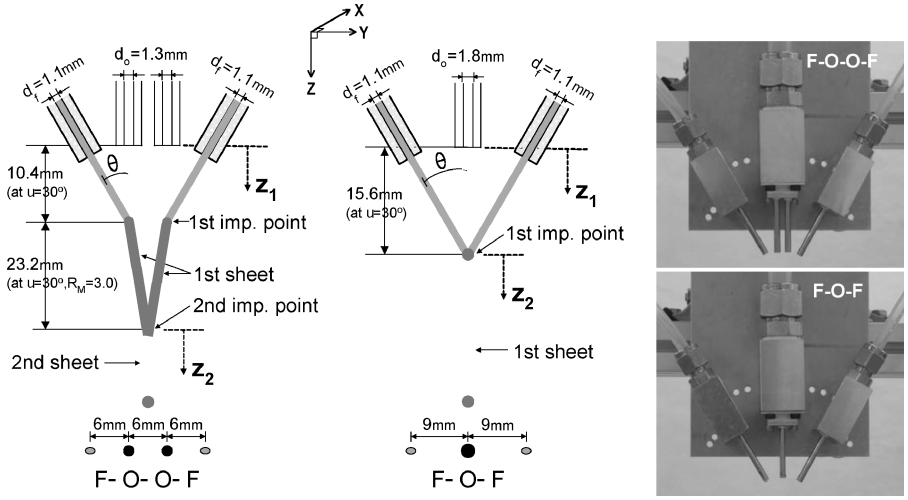

Fig. 3 Schematics of F–O–O–F and F–O–F injectors for present study and photographs of injector assemblies: inner oxidizer orifice(s) and outer fuel orifices.

Table 1 Mass flow rates and injection velocities of the present simulants for the similarity of momentum ratio of LOX/kerosene propellant

Momentum ratio R_M	0.5	1.0	1.5	2.0	2.5	3.0[a]	3.5	4.0	4.5	5.0	5.5	6.0	6.5
Mass flow rate $\dot{M}$, g/s													
$\dot{M}_o$	13.1	18.5	22.7	26.2	29.3	32.1	34.6	37.0	39.3	41.4	43.4	45.3	47.2
$\dot{M}_f$	16.0	16.0	16.0	16.0	16.0	16.0	16.0	16.0	16.0	16.0	16.0	16.0	16.0
Injection velocity V, m/s													
V_o	5.1	7.3	8.9	10.3	11.5	12.6	13.6	14.6	15.4	16.3	17.1	17.8	18.5
V_f	8.4	8.4	8.4	8.4	8.4	8.4	8.4	8.4	8.4	8.4	8.4	8.4	8.4

[a]Design momentum ratio corresponding to the mixture ratio of 2.3 for LOX/kerosene propellant.

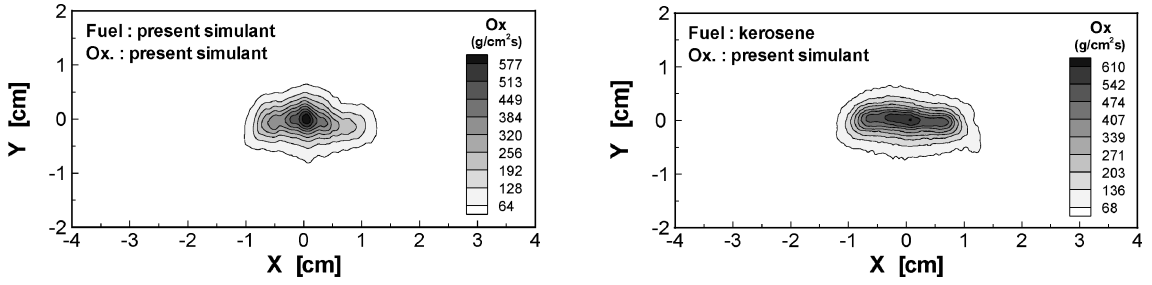

a) Present simulant as a fuel **b) Kerosene as a fuel**

Fig. 4 Oxidizer mass distributions of F–O–O–F injector when using the present simulant or kerosene were used as a fuel ($2\theta = 60$ deg, $R_M = 3.0$, and $Z_1 = 5$ cm).

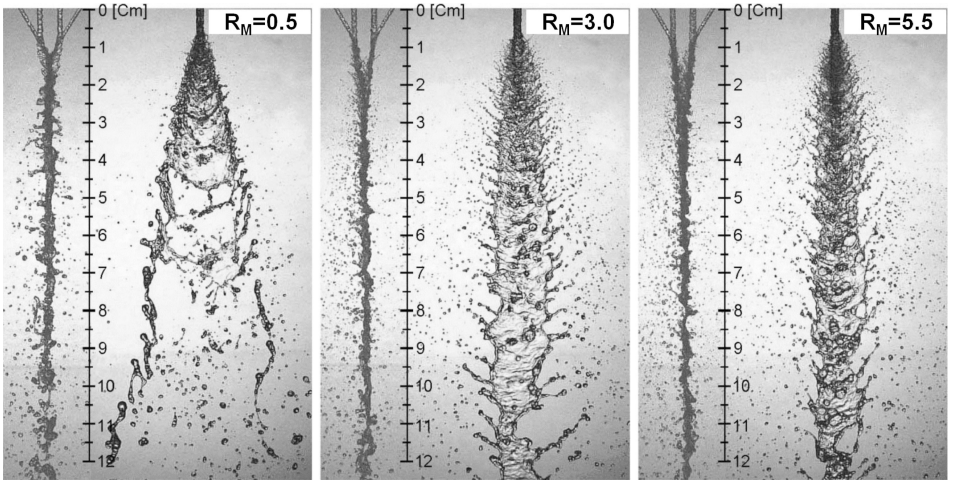

a) F–O–O–F injector

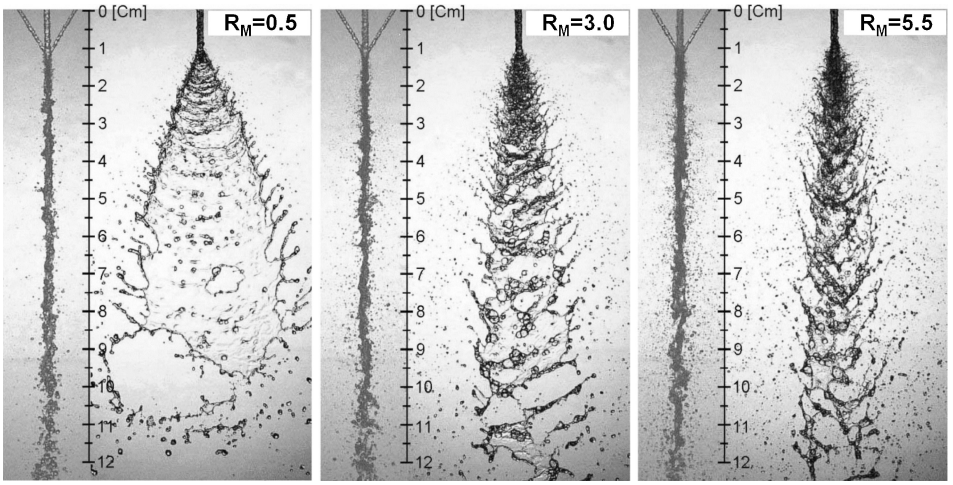

b) F–O–F injector

Fig. 5 Spray patterns of a) F–O–O–F and b) F–O–F injectors as a function of momentum ratio of oxidizer to fuel R_M ($2\theta = 60$ deg).

distributions of the oxidizer obtained by the PLLIF technique. The present simulant and kerosene were used as fuel in Figs. 4a and 4b, respectively, under the same momentum ratio of 3.0. The results showed no significant difference in the absolute value, nor in the distribution shape of oxidizer mass. Consequently, the effects of liquid properties are not significant in the spray mass distributions only if the similarity of momentum ratio is satisfied.

III. Results and Discussion

A. Spray Pattern

Instantaneous images of Fig. 5 obtained with a stroboscope (with luminous time about 4 μs) show the spray patterns of the F–O–O–F and F–O–F injectors as a function of momentum ratio of the oxidizer to fuel. Figure 5 shows that the spray angles of the F–O–O–F injector are lower than those of the F–O–F injector for the same momentum ratio. Whereas the F–O–F injector forms the liquid sheet by the direct impingement of two fuel jets and one oxidizer, the F–O–O–F injector forms the final sheet at the second impingement point by the impingement of two liquid sheets formed by the first impingement of fuel and oxidizer jets. As a result, the impact force of the F–O–F injector is stronger than that of the F–O–O–F, and, thus, the spray angles of the F–O–F injector are higher than those of the F–O–O–F injector. From the result, the spray mass distribution of the F–O–O–F injector is expected to be more concentrated than that of the F–O–F at the spray center for the same momentum ratio, resulting in the different mixing efficiencies.

B. Mixing Mechanism at Design Condition

To understand the mixing mechanisms of both injectors, we used the following deviation indices (DI):

$$\mathrm{DI}_f[\%] = \frac{[\dot{m}_f - \dot{m}_o(\dot{M}_f/\dot{M}_o)]}{\dot{M}_o + \dot{M}_f} \times 100 \quad (r < R)$$

$$\mathrm{DI}_o[\%] = \frac{[\dot{m}_o - \dot{m}_f(\dot{M}_o/\dot{M}_f)]}{\dot{M}_o + \dot{M}_f} \times 100 \quad (r \geq R) \tag{5}$$

The indices indicate the deviation of local mass flow rate from the ideal mass flow rate, for example, the DI_f is calculated as the ratio of the difference between actual and ideal mass flow rates of fuel to the total injected mass flow rate at fuel-rich mass flow rates ($r < R$).

Figure 6 shows the distributions of the DI for both injectors at the design conditions, that is, momentum ratio of 3.0 and impingement angle of 60 deg, as a function of measurement location. Because the mixing of fuel and oxidizer is dominated by the impingements of the jets, and the impingement locations of both injectors are not same, the measurement location was determined as the distance from the last impingement points of both injectors Z_2. The oxidizer-rich and fuel-rich regions were expressed as flood and line contours, respectively. Figure 6 shows large differences in the mixing processes as well as in the mass distributions of fuel and oxidizer. First, whereas the oxidizer-rich region of the F–O–O–F injector occupies the spray center except the case of 8 cm downstream, the fuel-rich region of the F–O–F injector is distributed at the spray center. In addition, whereas the spray area of the F–O–O–F injector is wider than that of the F–O–F injector, the x-axial spray length of the F–O–F injector is larger than that of the F–O–O–F injector at the same axial locations.

Figure 7 shows the mixing mechanisms of both injectors at the design momentum ratio based on Fig. 6; biases for the mass

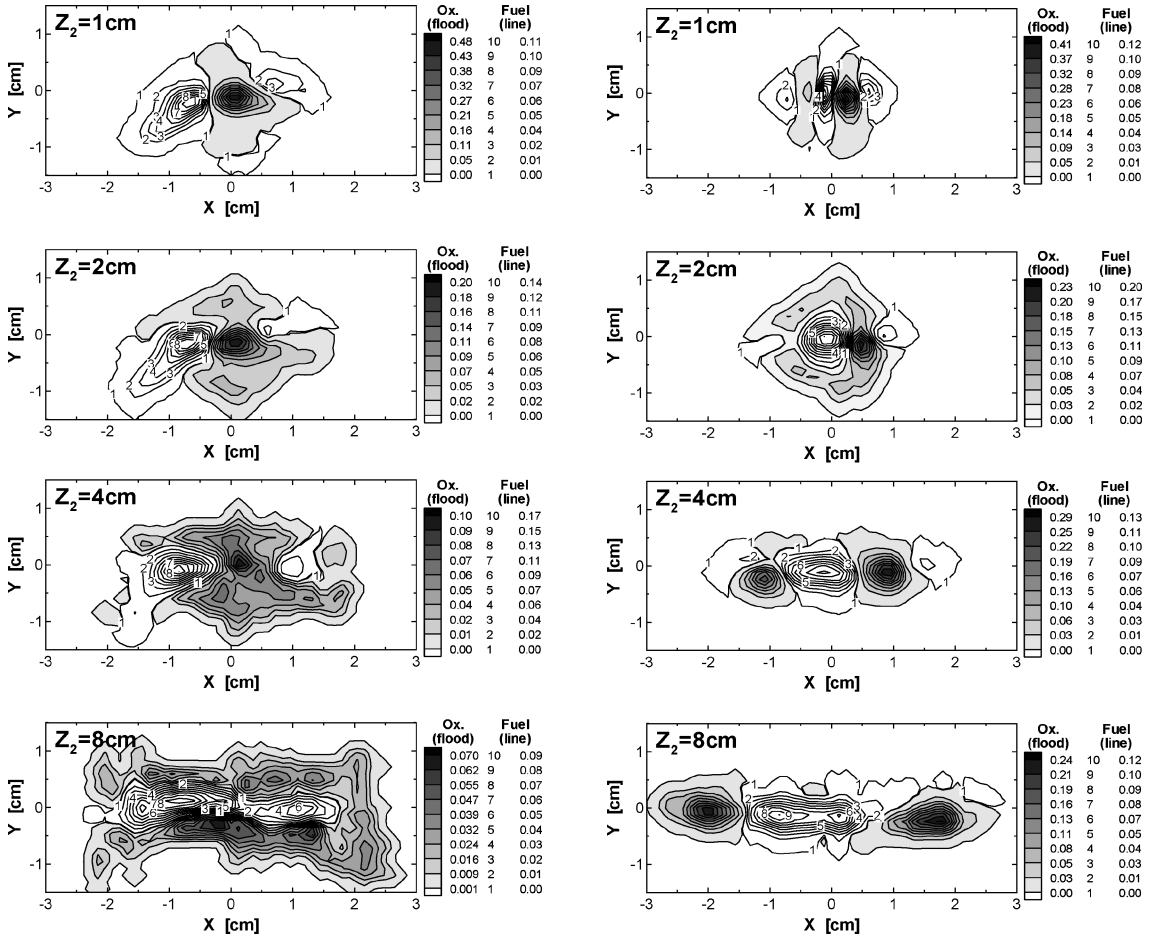

a) F–O–O–F injector b) F–O–F injector

Fig. 6 DI distributions of a) F–O–O–F and b) F–O–F injector sprays as a function of distance from last impingement point to measurement location Z_2; line and flood contours indicate fuel-rich and oxidizer-rich regions, respectively ($R_M = 3.0$ and $2\theta = 60$ deg).

concentrations of Fig. 6, which resulted from the misalignments of the injectors, were corrected in Fig. 7. The most important difference is the mixing mechanism of the fuel and oxidizer jets at the first impingement point. For the F–O–O–F injector, two pairs of fuel and oxidizer jets form two liquid sheets after their first impingements, and then the sheets move to the center with angles of δ because the reduction of the y-axial momentum by the first impingement is not so significant. As a result, the fuel and oxidizer do not mix well at the first impingement point, and, thus, the oxidizer-rich region forms at the center. Although the mixing of the F–O–O–F injector is improved by the second impingement, its impinging momentum is relatively low as compared with that of the F–O–F injector because the impingement of two liquid sheets of the F–O–O–F injector is weaker than that of the liquid jets of the F–O–F injector, and, thus, the oxidizer of the F–O–O–F injector is still distributed at the spray center even after the second impingement, as shown in Figs. 6a and 7. Contrary to the F–O–O–F injector, most of the y-axial momentums of two fuel jets of the F–O–F injector are lost after their impingements with the oxidizer jet. Instead, the fuel jets penetrate into the oxidizer jet during the process so that the oxidizer is separated into two parts, and the fuel is distributed at the spray center as shown in Figs. 6(b) and 7. Therefore, it is expected that the mixing of fuel and oxidizer of the F–O–F injector is better than that of the F–O–O–F injector because the penetrations of fuel jets of the F–O–F injector are stronger than those of the F–O–O–F injector.

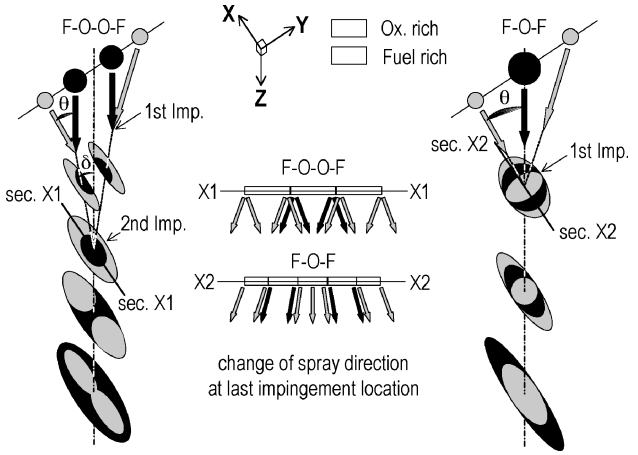

Fig. 7 Mixing processes and efficiencies of F–O–O–F and F–O–F injectors as function of measurement location ($R_M = 3.0$ and $2\theta = 60$ deg).

Another important difference in the mixing process is the spray directions of fuel and oxidizer after the last impingement locations of both injectors. As shown in Fig. 7, the three liquid jets of the F–O–F injector collide at one point and form one liquid sheet that has only a radial flow direction from the impingement point. As a result, the outer oxidizer-rich zone is separated from the central fuel-rich region after 4 cm downstream from the second impingement point, as shown in Fig. 6b. In contrast to the F–O–F injector, the F–O–O–F injector has a number of impingement points on the impingement line of two liquid sheets, and the points can make local sheets that have radial flow direction. When it is considered that the final sheet results from the superposition of the local sheets, the outer fuel-rich and the central oxidizer-rich zones of the F–O–O–F injector can have both x^- and x^+ directions after the second impingement. As a result, both zones spread, and, finally, the outer fuel-rich zones are merged at the center, as in the case 8 cm downstream shown in Fig. 6a.

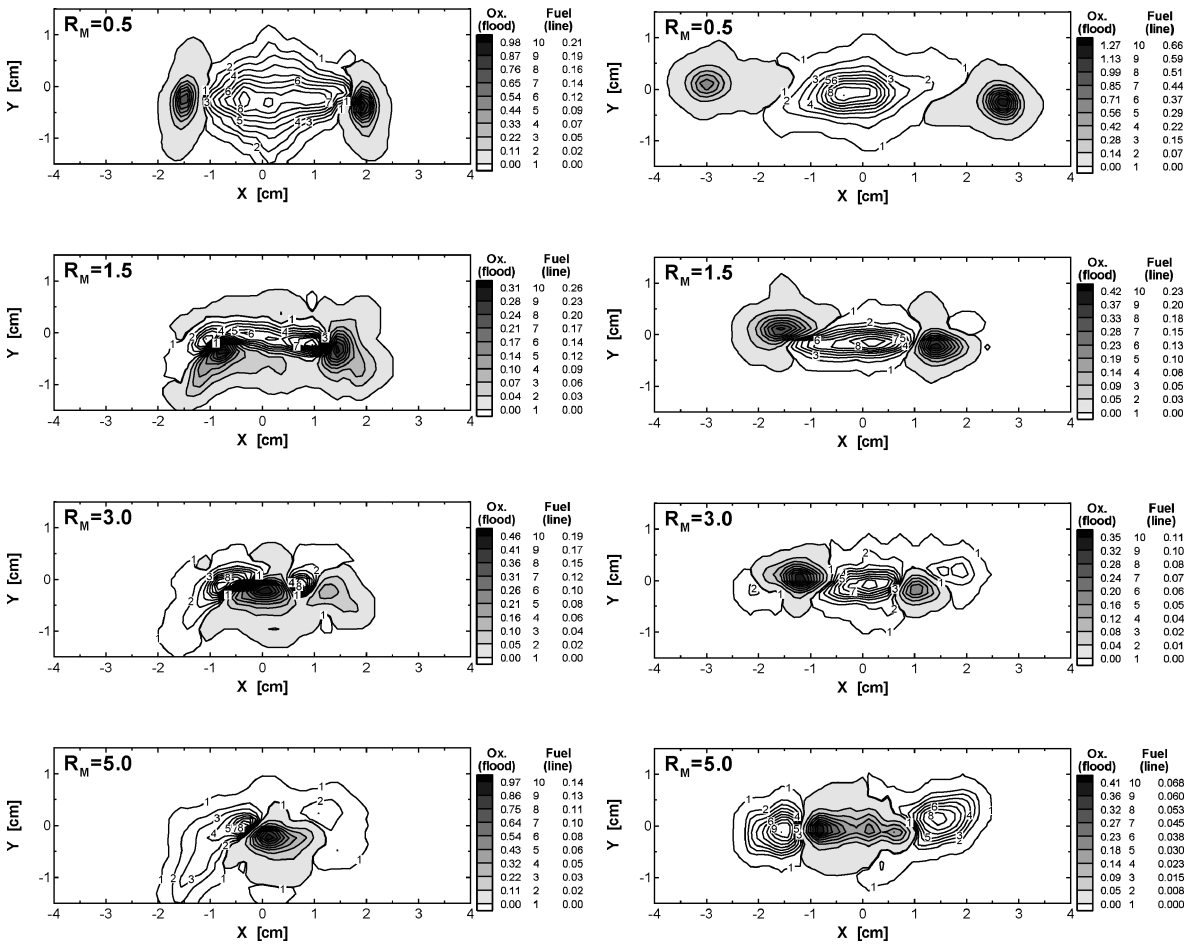

a) F–O–O–F injector **b) F–O–F injector**

Fig. 8 DI distributions of the a) F–O–O–F and b) F–O–F injectors as function of momentum ratio of oxidizer to fuel R_M ($2\theta = 60$ deg and $Z_1 = 6$ cm).

C. Momentum Ratio Effects on Mixing Efficiency

To compare the mixing performance between the F–O–O–F and F–O–F injectors quantitatively, we calculated mixing efficiencies at the transverse plane of spray as follows[4]:

$$E_m = 100 - \left[\sum_0^n \mathrm{DI}_f + \sum_0^n \mathrm{DI}_o \right] \tag{6}$$

Equation (6) indicates that the mixing efficiency decreases as the deviation of the mass flow rate (DI_f or DI_o) or the area of the fuel- or oxidizer-rich zone (n or $\bar{n}$) increases in percentage.

Figures 8 and 9 show the distributions of mass flow rate deviations and the changes of mixing efficiency at the fixed 6-cm downstream location from the injector surface as the momentum ratio of oxidizer to fuel varies. The measurement locations of both injectors were determined to be the same to compare their mixing performances at a given location, and the 6-cm location includes all of the impingement points, especially for the case $R_M = 6.5$ (about 5.5 cm from the surface of the F–O–O–F injector). In the cases of a low momentum ratio of 0.5, the fuel jets separate the oxidizer regions with their high momentums, as shown in Fig. 8, and these separations cause the mixing efficiencies of both injectors to decrease, as shown in Fig. 9. However, that the mixing efficiency of the F–O–F injector (12%) is much lower than that of the F–O–O–F injector (58%). This results from the deviations of both the fuel-rich and oxidizer-rich zones of the F–O–O–F injector being lower than those of the F–O–F injector because the oxidizer-rich zone of the F–O–O–F injector is less separated from the spray center by the lower impinging momentum, as shown in Fig. 8.

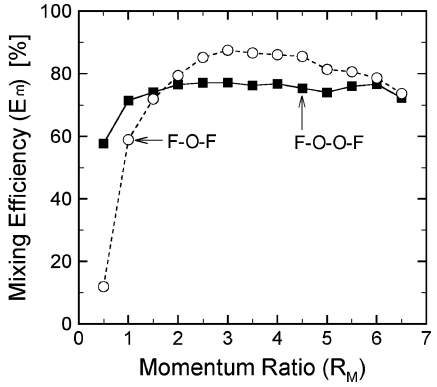

Fig. 9 Mixing efficiencies of ■, F–O–O–F and ○, F–O–F injectors as function of momentum ratio of oxidizer to fuel R_M ($2\theta = 60$ deg and $Z_1 = 6$ cm).

As the momentum ratio of oxidizer to fuel increases, the impinging momentum of the fuel jets decreases relatively, so that the central fuel-rich zones are converted into oxidizer-rich zones. From Fig. 8, it can be estimated that the convertion processes of the F–O–O–F and F–O–F injectors occur when the momentum ratios are about 2.0 and 4.0, respectively. It is thought that the result that the converting momentum ratio of the F–O–O–F injector is lower than that of the F–O–F injector also results from the lower second impinging momentum of the F–O–O–F injector.

The most important result of Fig. 9 is that the mixing efficiency of the F–O–O–F injector is not affected by the momentum ratio significantly. This is a remarkable feature of the F–O–O–F injector; generally, the mixing performances of common injectors decrease as the operating range of mixture ratio becomes farther from the design mixture ratio, especially in starting injection,[5] but the F–O–O–F injector is expected to have stable mixing performance for the wide operating range. This also may result from the difference in the impingement mechanisms; that is, because the mixing of the F–O–O–F injector is based on the coalescing process of two liquid sheets, the mixing efficiency is less sensitive to the impinging momentum of the first impingement location. Although the mixing efficiency of the F–O–F injector is more sensitive to the momentum ratio than that of the F–O–O–F injector, it is about 10% higher than that of the F–O–O–F when the momentum ratio is close to the design condition of 3.0 because the mixing caused by the jet impingements is more efficient than that by the sheet impingement.

D. Impingement Angle Effects on Mixing Efficiency

From the results of the momentum ratio, it was found that the strong impinging momentums of fuel jets can assist in mixing with

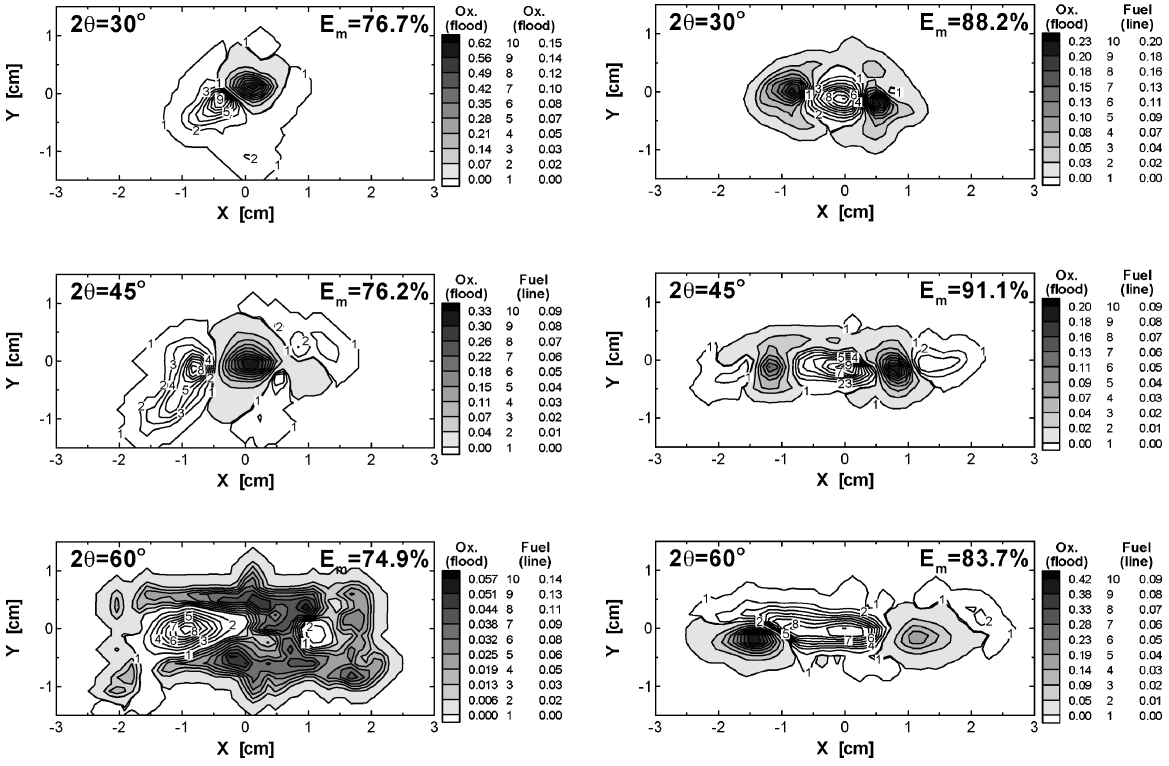

a) F–O–O–F injector **b) F–O–F injector**

Fig. 10 DI distributions and mixing efficiencies of a) F–O–O–F and b) F–O–F injectors as function of impingement angle 2θ ($R_M = 3.0$ and $Z_1 = 8$ cm).

the oxidizer, but the excessive momentums may separate the oxidizer at the spray center and reduce the mixing efficiency, especially for the F–O–F injector. Because the impinging momentum of the fuel is also increased by the increase of the impingement angle 2θ, we investigated the effects of the impingement angle on the mixing performance.

Figure 10 shows the distributions of mass flow rate deviations and the mixing efficiencies for both injectors at the fixed 8-cm downstream location from the injector surface as the impingement angle is varied; the 8-cm location includes all of the impingement points, especially at $2\theta = 30$ deg (about 6.7 cm from the surface of F–O–O–F injector). As for the F–O–F injector, the mixing of fuel and oxidizer is improved by the increase of the impinging momentum of fuel until 45 deg, but the momentum becomes strong enough to separate the oxidizer-rich region, reducing the mixing efficiency by about 7% at the impingement angle of 60 deg. In contrast, the mixing efficiency of the F–O–O–F injector decreases as the impingement angle increases, but the decrement is not as significant as compared with that of the F–O–F injector. The reason is that, although the area of the oxidizer-rich zone of the F–O–O–F injector becomes very large at the angle of 60 deg, the low deviations of oxidizer mass flow rate compensate for the mixing efficiency, and, thus, the efficiency does not decrease significantly. In other words, the F–O–O–F injector can have a very uniform mixing distribution without the loss of mixing efficiency at the high impingement angle, such as 60 deg, which is too high for the F–O–F injector.

IV. Conclusions

In the present study, the two-dimensional mass distributions of oxidizer and fuel were measured by using the PLLIF technique, and the mixing characteristics of F–O–O–F and F–O–F injectors were compared. From the results, the following conclusions are drawn:

1) The impinging momentum of the F–O–O–F injector is lower than that of the F–O–F injector because the impingement of two liquid sheets of the F–O–O–F injector at the second impingement location is weaker than that of three liquid jets of the F–O–F injector. Therefore, the mixing efficiency of the F–O–O–F injector is lower than that of the F–O–F injector at the same injection conditions.

2) The strong impinging momentums of fuel jets assist in the mixing of the jets with the oxidizer jet, but excessive momentums can separate the oxidizer at the spray center and reduce the mixing efficiency, especially in the case of the F–O–F injector. As for the F–O–O–F injector, because the mixing is determined by the coalescing process of the two liquid sheets rather than the jet impingements, and the impinging momentum of two sheets is weak, the mixing efficiency is less sensitive to the momentum ratio of oxidizer to fuel.

3) As for the F–O–O–F injector, the area of the oxidizer-rich zone becomes larger as the impingement angle increases, but the lower deviations of the oxidizer mass flow rate compensate for the mixing efficiency variation, and, thus, the F–O–O–F injector shows a uniform mixing distribution without the loss of mixing efficiency. On the other hand, the mixing of the F–O–F injector is improved by the increase of the impingement angle, but the excessive impinging momentum of fuel jets due to the increase of the angle can separate the oxidizer-rich zone and reduce the mixing efficiency.

Acknowledgment

This research was supported by the KSR-III project and National Research Laboratory Program (M1-0104-00-0058). The authors wish to acknowledge this financial support.

References

[1]Harrje, D. T., and Reardon, F. H., "Liquid Propellant Rocket Combustion Instability," NASA Rept. SP-194, 1972.

[2]Pieper, J., Nguyen, T., and Hulka, J., "Performance and Stability Characterization of Liquid Oxygen/Kerosene Injectors at Aerojet," *Recent Advances in Spray Combustion: Spray Combustion Measurements and Model Simulation*, Vol. 2, Progress in Astronautics and Aeronautics, AIAA, Washington, DC, 1995, pp. 349–368.

[3]Gill, G. S., and Nurick, W. H., "Liquid Rocket Engine Injectors," NASA Rept. SP-8089, March 1976.

[4]Frrenberg, A., Hunt, K., and Duesberg, J., "Atomization and Mixing Study," NASA CR-178751, Dec. 1985.

[5]Sutton, G. P., *Rocket Propulsion Elements*, Wiley-Interscience, New York, 1992, Chap. 4.

[6]Pavli, A. J., "Design and Evaluation of High Performance Rocket Engine Injectors for Use with Hydrocarbon Fuels," NASA TM-79319, 1979.

[7]Won, Y. D., Cho, T. H., and Yoon, W. S., "Effect of Momentum Ratio on the Mixing Performance of Unlike Split Triplet Injectors," *Journal of Propulsion and Power*, Vol. 18, No. 4, 2002, pp. 847–854.

[8]Rupe, J. H., "A Correlation Between the Dynamic Properties of a Pair of Impinging Streams and the Uniformity of Mixture-Ratio Distribution in the Resulting Spray," Jet Propulsion Lab., California Inst. of Technology, Rept. 20-209, Pasadena, CA, March 1956.

[9]Bachalo, W. D., and Houser, M. J., "Phase/Doppler Spray Analyzer for Simultaneous Measurement of Drop Size and Velocity Distributions," *Optical Engineering*, Vol. 23, No. 5, 1984, pp. 583–590.

[10]Ruff, G. A., and Faeth, G. M., "Non-intrusive Measurement of the Structure of Dense Sprays," *Recent Advances in Spray Combustion: Spray Combustion Measurements and Model Simulation*, Vol. 1, Progress in Astronautics and Aeronautics, AIAA, Washington, DC, 1995, pp. 263–296.

[11]Brown, C. T., McDonell, V. G., and Talley, D. G., "Accounting for Laser Extinction, Signal Attenuation, and Secondary Emission While Performing Optical Patternation in a Single Plane," *ILASS Americas 15th Annual Conference on Liquid Atomization and Spray Systems*, ILASS Americas, Madison, WI, 2002.

[12]Le Gal, P., Farrugia, N., and Greenhalgh, D. A., "Laser Sheet Dropsizing of Dense Sprays," *Optical and Laser Technology*, Vol. 31, 1999, pp. 75–83.

[13]Jung, K., Koh, H., and Yoon, Y., "Assessment of PLLIF Measurement for Spray Mass Distribution of Like-Doublet Injector," *Measurement Science and Technology*, Vol. 14, No. 8, 2003, pp. 1387–1395.

[14]Dombrowski, N., and Hooper, P. C., "A Study of the Sprays Formed by Impinging Jets in Laminar and Turbulent Flow," *Journal of Fluid Mechanics*, Vol. 18, 1964, pp. 392–400.

[15]Riebling, R. W., "Criteria for Optimum Propellant Mixing in Impinging-Jet Injection Elements," *Journal of Spacecraft and Rockets*, Vol. 4, No. 6, 1967, pp. 817–819.